Facile fabrication of polyaniline films with hierarchical porous networks for enhanced electrochemical activity

Ji-Hye Kim[a,1], Ju-Hee So[b,1], Sung-Kon Kim[c], Hyunsik Yoon[a], Jonghoon Choi[d], Hyung-Jun Koo[a,*]

[a] Department of Chemical and Biomolecular Engineering, Seoul National University of Science and Technology, Seoul, 01811, Republic of Korea
[b] Research Institute of Industrial Technology Convergence, Korea Institute of Industrial Technology, Ansan, 15588, Republic of Korea
[c] School of Chemical Engineering, Jeonbuk National University, Jeonju, 54896, Republic of Korea
[d] School of Integrative Engineering, Chung-Ang University, Seoul, Republic of Korea

ABSTRACT

This paper describes a facile method for fabricating polyaniline (PANI) films with well-defined three-dimensional (3D) porous networks and improved electrochemical activity. The PANI hydrogel pastes with different compositions are directly cast into thin films by the doctor blade technique. After a dehydration step, the conductivity of the PANI drastically increases, while the porous structure with hierarchical macro- and meso-porosity is formed in the PANI film. The electrical conductivity tends to increase with the thickness of the porous PANI film until it fails to form a mechanically stable film not exhibiting cracking problems. We found that the amount of the initiator, the aniline monomer, and the crosslinker significantly affect not only the micro-morphology of PANI films, but also their electrical and electrochemical characteristics. Importantly, when the amounts of the crosslinker and the initiator increase, the polymer film forms with a dense internal morphology with smaller pores. Based on the engineered synthesis composition, we demonstrate a supercapacitor with porous PANI electrodes. Due to the hierarchical porous structure, large surface area and the improved conductivity, the resulting devices show excellent volumetric capacitances, which are comparable to or much higher than those previously reported.

© 2020 The Korean Society of Industrial and Engineering Chemistry. Published by Elsevier B.V. All rights reserved.

Introduction

Technologies that control the morphology and physicochemical properties of conductive polymers have attracted increased attention in improving their processability and the performance of the resulting functional devices [1–9]. The ability to engineer the material properties in moderate environments (e.g., low temperature and atmospheric pressure) with low costs allows the conductive polymers to be used for a variety of applications including membranes, diodes, sensors, electrochemical cells, and printed electronic circuits [10–15]. In particular, the conductive polymer with a well-defined pore structure can be applied in many electrochemical applications, as the porous network with a large surface area plays a crucial role in facilitating the transport and access of ions to the interfacial area containing the electrolytes.

There are several different approaches for embodying porous polymer structures, including self-assembly [16], crosslinking [17,18], the freeze-drying process [19,20], the incorporation of porogen materials [21], use of supercritical fluids [22,23], and colloidal templating [24–26].

Polyaniline (PANI) is one of the most widely investigated conductive polymers as it has the advantages of a relatively high electrical conductivity, simple synthesis procedure, and ease of forming composites with other types of materials such as metal nanoparticles and carbon based nanomaterials [27]. Especially, due to its electrochemical activity on the surface, PANI has been actively adopted as an active material for chemical sensors [28,29], pseudocapacitors [30–33], etc [34,35]. In 2012, a novel, simple process to fabricate a PANI hydrogel with well-defined micropores was reported [36]. In the process, the initiator solution is mixed with the second solution containing the aniline monomer and phytic acid where the phytic acid serves as both a crosslinker and a doping agent. One interesting characteristic of the PANI hydrogel is its three-dimensionally distributed porous structure. Aniline monomers are crosslinked by phytic acid and form a PANI hydrogel

with a three-dimensionally interconnected PANI nanofiber network. The highly conductive electrical properties and porous structure of the PANI hydrogel enable it to be used as the electrode material of electrochemical devices such as supercapacitors. Importantly, the moderate viscosity of the hydrogel phase endows the PANI with better processability, enabling ink-jet printing, doctor-blading, screen printing and stencil lithography. Moreover, the dehydration of the PANI hydrogel improved the electrical conductivity, while maintaining the hierarchical porous structure. The synthetic composition of the PANI hydrogel probably has a significant influence on the pore morphology and physicochemical properties of the dried PANI film. However, such study has not been systematically conducted yet.

In this paper, we present a facile process for fabricating a porous PANI film with very high electrical conductivity by using the ways in which the synthetic compositions of PANI hydrogel paste can affect the morphology and electrical property of the resulting PANI film. The PANI film was formed by a doctor-blading technique with the viscous PANI hydrogel paste. The doctor blading technique is one of the simple and efficient methods to form a thin film. In the technique, the film thickness can be easily controlled by adjusting the gap between the substrate and the blade. The technique is very versatile by which various materials can be deposited as long as they have appropriate viscosity. We confirmed that the thicker and more dehydrated the PANI film, the higher the conductivity. To investigate the effects of the synthetic composition on the properties of the PANI film, we varied the amounts of initiator, monomer, and crosslinker and then compared the surface morphology and the electrical conductivity. The resulting porous PANI films can be used to improve the performance of electrochemical devices by utilizing the highly conductive porous structures as electrodes where electrochemical reactions occur. To compare the electrochemical performances of the PANI film with different compositions, we fabricated a 3-electrode electrochemical setup using the PANI film as a working electrode and analyzed the electrochemical characteristics through cyclic voltammetry (CV), galvanostatic charge-discharge (GCD), and electrochemical impedance spectroscopy (EIS). We also fabricated a two-electrode capacitor with symmetric PANI electrodes and discuss its performance and operational stability.

Experimental section

Materials

Aniline ($\geq$99.5%), phytic acid solution (50 wt% in H_2O), and ammonium persulfate ($\geq$98.0%), were purchased from Sigma–Aldrich Korea (South Korea) and sulfuric acid (H_2SO_4, 95.0%) was purchased from Samchun Pure Chemicals (South Korea). The chemicals were used without any further treatment or purification. A filter paper was purchased from Toyo Roshi Kaisha, Ltd. (Japan) and was used as the separator of the supercapacitor. The grade of the filter paper is No.131 (the pore size is 3 μm, and its thickness is 0.25 mm). De-ionized (DI) water was obtained from the ultrapure water production unit (Milipore/direct-Q3UV, FR/DIRECT-Q3UV, USA). Silver paste was purchased from Chemical Aerosol Network System (CANS, Japan).

Preparation and characterization of PANI porous films

The PANI hydrogel paste was prepared by referring to processes described in previously published literature [36]. In brief, the aqueous solution of ammonium persulfate (the initiator), and the aqueous solution of aniline (the monomer) and phytic acid (the crosslinker and dopant) were prepared and stored at 4 °C. The two aqueous solutions were mixed thoroughly in a vial using a vortex mixer for 20–30 s until the color of the mixture turned dark green. The mixture was poured into a petri dish, becoming a PANI hydrogel paste. The hydrogel paste was immersed in DI water for over 5 h, while the water was replenished every hour to fully remove any remaining unreacted materials. To investigate the effects of the composition of the hydrogel paste on the conductivity and the film morphology of the PANI porous film, we varied the amounts of each component. We chose 1.25 mmol of the initiator, 5 mmol of the monomer, and 1 mmol of the crosslinker in 3 ml of water, as used in earlier study [36], as a "reference (REF) composition".

The fabrication method of the porous PANI film is shown in Fig. 1. The prepared PANI hydrogel paste was deposited by a doctor-blade technique on a glass substrate, followed by being dried at room temperature (20–25 °C) for a minimum of 30 min until the color of the film turned cyan. The typical dimensions of the films were 0.6 cm × 1.9 cm. The thickness of the PANI film was controlled by the number of layers of an adhesive tape (50 μm in thickness, Scotch® Magic™ tape, 3 M, USA) used as a spacer in the doctor-blade technique. The conductivity of the PANI films was measured using a sourcemeter (Keithley 2450, Tektronix, USA). The surface morphology and the thickness of the PANI porous films were characterized by a scanning electron microscope (SEM) (coxem, EM-30, South Korea). The surface area and pore characteristics of the PANI film were measured by using a multiport chemisorption/physorption/micropore analyzer (Micromeritics, 3flex, USA). Each sample was measured in powder form after undergoing heat
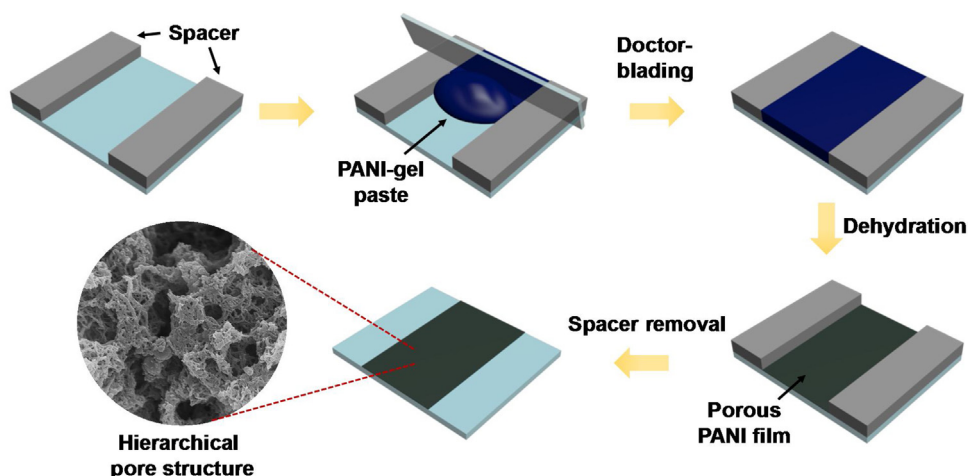

Fig. 1. Fabrication process of the PANI film with a hierarchical porous network by direct doctor-blading of a PANI-gel paste.

treatment at 150 °C overnight. The pore size distributions were measured by using a pore characterizing system (Micromeritics, AutoPore 9520, USA), and the pressure applied was from 0.5 to 60,000 psi.

Electrochemical measurements

For measurement of capacitive performance, the PANI hydrogel paste was applied using the doctor-blade technique on a platinum plate as a current collector and dried for 30 min. The area and thickness of the dried PANI porous electrodes were ~0.25 cm^2 and ~21 μm, respectively. The electrochemical characterizations including cyclic voltammetry (CV), galvanostatic charge/discharge (GCD), and electrochemical impedance spectroscopy (EIS) were performed using a single channel Potentiostat/Galvanostat (Bio-Logic, SP-200) in both the three- and two-electrode configurations. In the three-electrode configuration, the PANI electrode was used as a working electrode with a Ag/AgCl reference electrode and a platinum wire counter electrode in 0.1 M of H$_2$SO$_4$ aqueous solution over the potential range of −0.2 to 0.8 V at different scan rates. The EIS measurement was carried out in frequencies ranging from 10^6 Hz to 10^{-2} Hz at AC voltage amplitude by applying a 10 mV signal. For the two-electrode configuration, two PANI electrodes were assembled with a filter paper as a separator, which was soaked into 0.1 M of H$_2$SO$_4$ aqueous electrolyte. The volumetric capacitances (C$_v$) were calculated by using the following Eqs. (1) and (2), for the three- and two-electrode configurations, respectively.

$$C_{V,three} = \frac{\Delta t \cdot I}{\Delta V \cdot V} \tag{1}$$

$$C_{V,two} = 4 \times \frac{\Delta t \cdot I}{\Delta V \cdot V} \tag{2}$$

where $\Delta t/\Delta V$ is the slope of the discharge curve after an IR drop at the beginning of the discharge curve, I is the applied discharge current and V is the total volume of the PANI electrodes. The volumetric capacitance for the three-electrode configuration was also obtained by integrating the CV curves as follows:

$$C_{V,CV} = \frac{\int I \cdot dV}{\upsilon \cdot \Delta V \cdot V} \tag{3}$$

where $\int (I \cdot dV)$ is the integral area of the CV graphs, υ is the scan rate, ΔV is the voltage window and V is the volume of the PANI electrode.

Results and discussion

The dehydration of the PANI hydrogel film could increase the film density, thereby increasing its electrical conductivity. We synthesized a PANI hydrogel paste with the REF composition (1 mmol of crosslinker, 1.25 mmol of initiator, and 5 mmol of monomer), then deposited on a glass substrate using the doctor-blade technique to form PANI films. Fig. S1 shows the change in the conductivity and the thickness of the PANI films during dehydration for 50, 150, 250 and 350 μm initial thicknesses. For all the PANI films, the resistance decreases with the dehydration time until 30 min have elapsed and then levels off afterward. The conductivity of the PANI hydrogel films with different thicknesses, before and after dehydration, is compared in Fig. 2 (a). The conductivity increases by 60~130 times after dehydration with the exception of the 350 μm thick sample. The conductivity values of the dried PANI films are 0.67~0.91 S/cm, which is higher than the previously reported value for the dried PANI powder (0.23 S/cm) [36]. The reason for the increased conductivity of the dried PANI films when
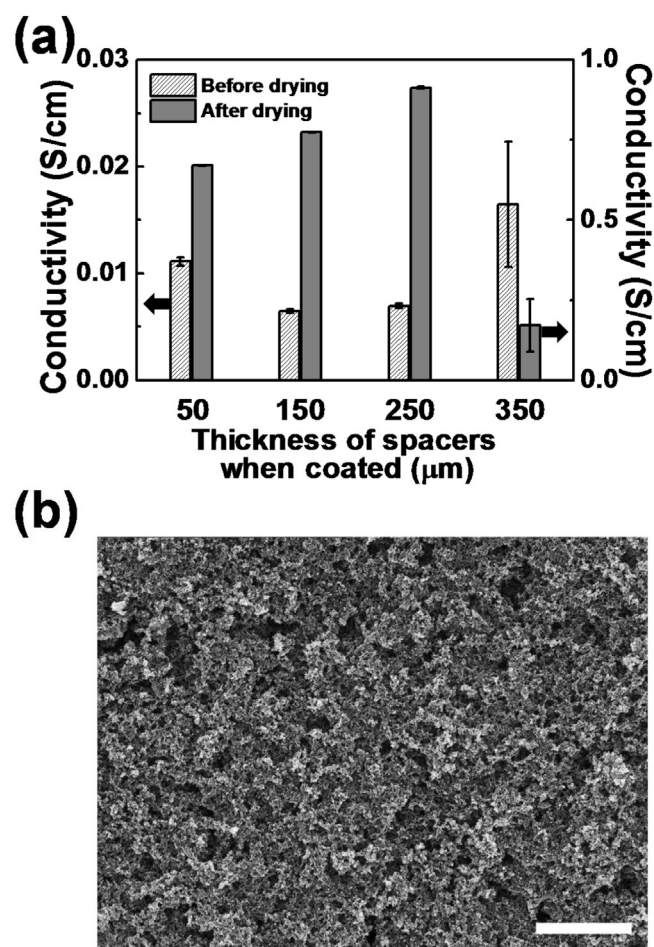

Fig. 2. (a) Conductivity of PANI films with different initial thicknesses before and after drying for 120 min. (b) SEM image of the PANI film. The PANI films in (a) and (b) were prepared with the REF composition (1 mmol of crosslinker, 1.25 mmol of initiator, and 5 mmol of monomer). Scale bar represents 10 μm.

compared to their wet state is that the distances between the PANI polymer chains are decreased as the water molecules evaporate. Indeed, the thickness of the PANI film after dehydration drastically decreases (Fig. S1 (b)). Interestingly, the conductivity of the dried PANI films slightly increases with the initial film thickness from 50 μm to 250 μm, which may suggest that the internal structure of the films with different thicknesses are not identical. It should be noted that the ratio of decrease for the PANI films with 50 and 250 μm are 82% and 91.5%, respectively. As the thickness increases, the polymer chains are likely to be more densely packed during dehydration, resulting in the increase in the electrical conductivity. When the initial film thickness further increases to 350 μm, the degree of volume shrinkage of the film during dehydration is too large, which causes formation of cracks (Fig. S2) and leads to a drastic decrease in the conductivity. After the drying process, the PANI film contains the porous structure, as shown in Fig. 2 (b). Pores with various scales, from micron-sized macropores to submicron-sized mesopores are observed. The surface and pore characterization reveals the pore characteristics of ~25 m^2/g in specific surface area. Thus, the porous conducting polymer film based on the PANI hydrogel paste has been successfully prepared and the dehydration process effectively improves the film conductivity. The PANI hydrogel film having an initial thickness ranging between 150 and 250 μm shows good film stability and conductivity after dehydration.

In addition to the hydration level, the composition of polymer hydrogel could affect its morphology and conductivity [18,37,38]. We investigated how the relative amounts of the crosslinker, the monomer, and the initiator affect the physical morphology and conductivity of the PANI conductive films in wet and dried states. Fig. 3 (a) shows the conductivity of the PANI film depending on the amount of crosslinker (i.e. phytic acid), before and after the drying process. For the wet PANI film, the effect of the amount of the crosslinker on the conductivity of the film is not obvious, and the conductivity value is less reliable with a large standard deviation, compared to that of the dried state of the films. The conductivity of the dried PANI film increases with the amount of the crosslinker (Fig. 3 (a)), probably due to higher crosslinking density. Fig. 3 (b–e) compare the morphology of the porous PANI film prepared with small and large amounts of the crosslinker. The PANI film prepared with 1.5 mmol crosslinker (50% more than the REF composition) exhibits much denser film morphology with smaller pores than does the film with 0.75 mmol crosslinker (25% less than the REF composition). As the crosslinker content decreases, the PANI hydrogel paste becomes less viscous in a sol-like state, which also supports the effect of the crosslinker to increase the connection between the polymer chains. The conductivity of the PANI film, however, does not continually increase with the amount of the crosslinker. The conductivity of the PANI films stabilizes at amounts of crosslinker above 1.25 mmol. When the amount of the crosslinker is smaller than 0.50 mmol, the PANI hydrogel paste does not form a film with enough mechanical stability, presumably due to insufficient gelation.

Even though the morphology is different depending on the crosslinker content, the hierarchical porous structures with macro- and submicron-scale pores are well defined in cases with both low and high crosslinker contents, as shown in the magnified SEM images (Fig. 3 (c) and (e)). To confirm the hierarchical porous structure of the PANI films, the pore distribution was further characterized through mercury intrusion porosimetry (MIP) (Fig. 4). Pores with two different size regimes of $\sim$100 nm and in the tens of μm are observed even in the high crosslinker content, which is in good agreement with the SEM data. Such a hierarchical porous structure could enable the PANI film to be an efficient electrode for electrochemical systems due to the facilitated mass transfer.

The effect of the amount of aniline monomer is different than the effects exhibited by varying the amount of crosslinker. As the amount of monomer increases, the conductivity of the films tends to decrease for both wet and dry states (Fig. 5 (a)). In general, the molecular weight of polymers increases as monomer concentration increases [39,40]. When the amount of monomer is small, the polymers with short chain lengths form a dense film with small pores as shown in Fig. 5 (b), leading to high conductivity. As the
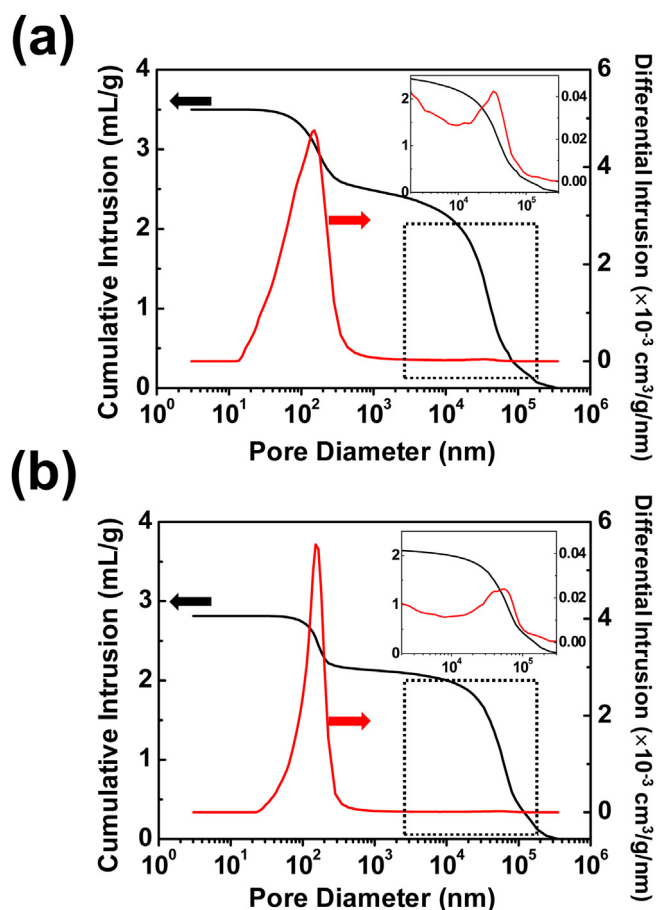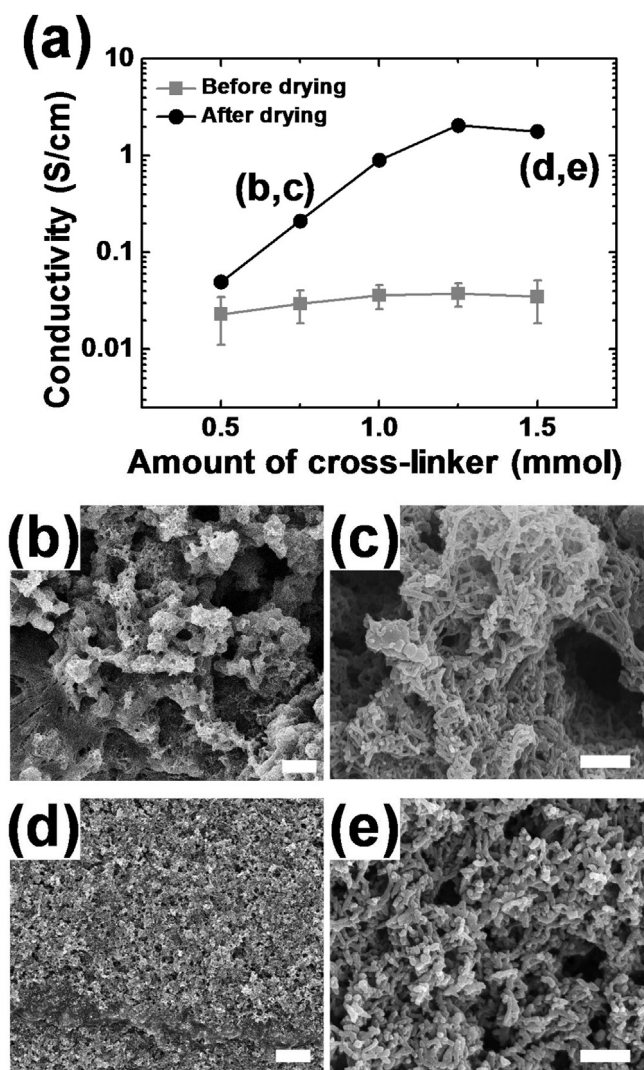

Fig. 3. Effect of the amount of the crosslinker, phytic acid. (a) Conductivity of the PANI film with the amount of the crosslinker before (■) and after (●) the dehydration process. SEM images of the PANI films with the crosslinker of (b,c) 0.75 mmol and (d,e) 1.5 mmol, whose conductivity values are indicated in (a). Scale bars = 10 μm (b,d) and 1 μm (c,e), respectively. All the porous PANI films were prepared with the 150 μm-thick spacer and then dried.

Fig. 4. Cumulative and differential pore volume distribution of PANI films with crosslinker of (a) 0.75 mmol and (b) 1.5 mmol. The regions indicated by the dotted line boxes are magnified in insets, to show the distribution of macropores.
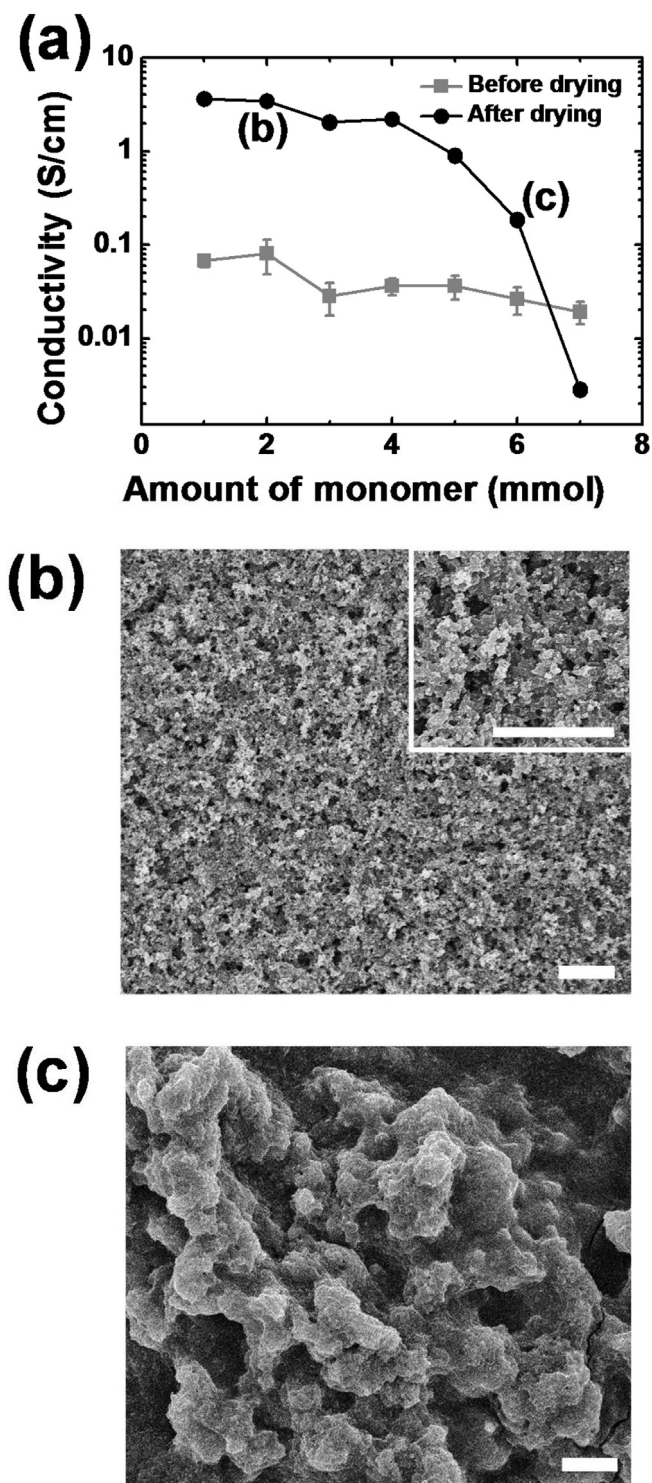
Fig. 5. Effect of the amount of the aniline monomer. (a) Conductivity of the PANI film with the amount of the monomer before (■) and after (●) the dehydration process. SEM images of the PANI films with the monomer of (b) 2 mmol and (c) 6 mmol, whose conductivity values are indicated in (a). Scale bars = 10 μm. All the porous PANI films were prepared with the 150 μm-thick spacer and then dried.

increase in the degree of phase separation in the solvent. It is known that as the molecular weight of polymers increases, entropy gain upon mixing becomes small and interaction between monomer segments in a polymer chain repel solvent molecules, leading to a higher degree of phase separation [41,42]. As a result, an agglomerated film morphology with larger pores is formed, leading to a decrease in conductivity.

The amount of initiator, ammonium persulfate, also influences the conductivity and morphology of the PANI film. The amount of initiator shows a similar effect to that of the crosslinker on the conductivity of the PANI films, that is, the conductivity increases with the amount of the initiator before drastically decreasing for amounts of initiator higher than 2.5 mmol (Fig. 6 (a)). When the film is wet, the conductivity tends to increase with the amount of initiator, contrary to its behavior when in its dried state. Fig. 6 (b) and (c) show the surface morphology of the PANI film at small and large amounts of initiator. As the amount of initiator increases, more polymer chains with low molecular weight form rather than increasing lengths of the polymer chains [43], resulting in the denser polymer networks. When the initiator is higher than a certain threshold amount of about 2.5 mmol, the conductivity decreases drastically due to the formation of cracks (white arrow in Fig. 6 (c)). This can be attributed to the high residual stress in the film caused by large volume shrinkage during the drying process. At low amounts of initiator, we anticipated that the coarse porous structure would form, similarly to the cases of small amounts of crosslinker or large amounts of monomer. Unexpectedly, the morphology of the PANI film manifests a relatively dense structure with small pores even at small amounts of initiator. (Fig. 6 (b)) Thus, the amount of initiator also affects the morphology and the conductivity of the PANI film, but not as much as that of monomer or crosslinker.

The PANI film with hierarchical 3D open pores and high surface area could be an efficient electrode for many electrochemical applications, especially as an electrode of a pseudocapacitor due to its reversible redox reaction. It was confirmed that the morphology of the porous PANI electrode changes with the monomer, initiator, and crosslinker compositions. As a result, the composition significantly affects the density, porosity, surface area, and therefore the electrochemical performance. To evaluate the electrochemical properties of the PANI film as an effective electrode, cyclic voltammetry (CV), galvanostatic charge-discharge (GCD), and electrochemical impedance spectroscopy (EIS) measurements in a 3-electrode configuration were performed. Fig. 7 (a) shows the CV curves of the PANI electrodes prepared at selected preparation compositions. Not surprisingly, two pairs of reversible redox peaks are observed in the potential readings at around 0 V and 0.2 V (resulting from the redox transition process from leucoemeraldine to emeraldine) and at 0.6 V and 0.8 V (resulting from redox transition from emeraldine to pernigraniline) [44]. The values of density, conductivity, volumetric surface area, and capacitances of the PANI films are summarized in Table 1. As expected, the C 1.5 and M 2 samples having a dense pore morphology (Figs. 3 (d) and 5 (b)) show higher film density and volumetric surface area than do other compositions. Notably, the C 1.5 PANI electrode exhibits the best volumetric capacitance of 330 F/cm^3, which is comparable to or even significantly higher than those of the PANI-based electrochemical electrodes recently reported [45–55]. This increased capacitance is due to well-developed hierarchical pore morphology and large volumetric surface area, as well as high electrical conductivity. Despite its high electrical conductivity, the PANI film prepared at the M 2 composition does not exhibit reliable CV curves. Since the PANI film tends to be mechanically weak as the monomer content decreases, the film prepared at lower monomer contents seems to

amount of monomer increases, the film morphology becomes coarser as shown in Fig. 5 (c), where very large macro-pores measuring tens of micrometers are observed. This morphology is caused by the increased molecular weight of the PANI polymer chains. The increase in the chain length of the PANI causes an
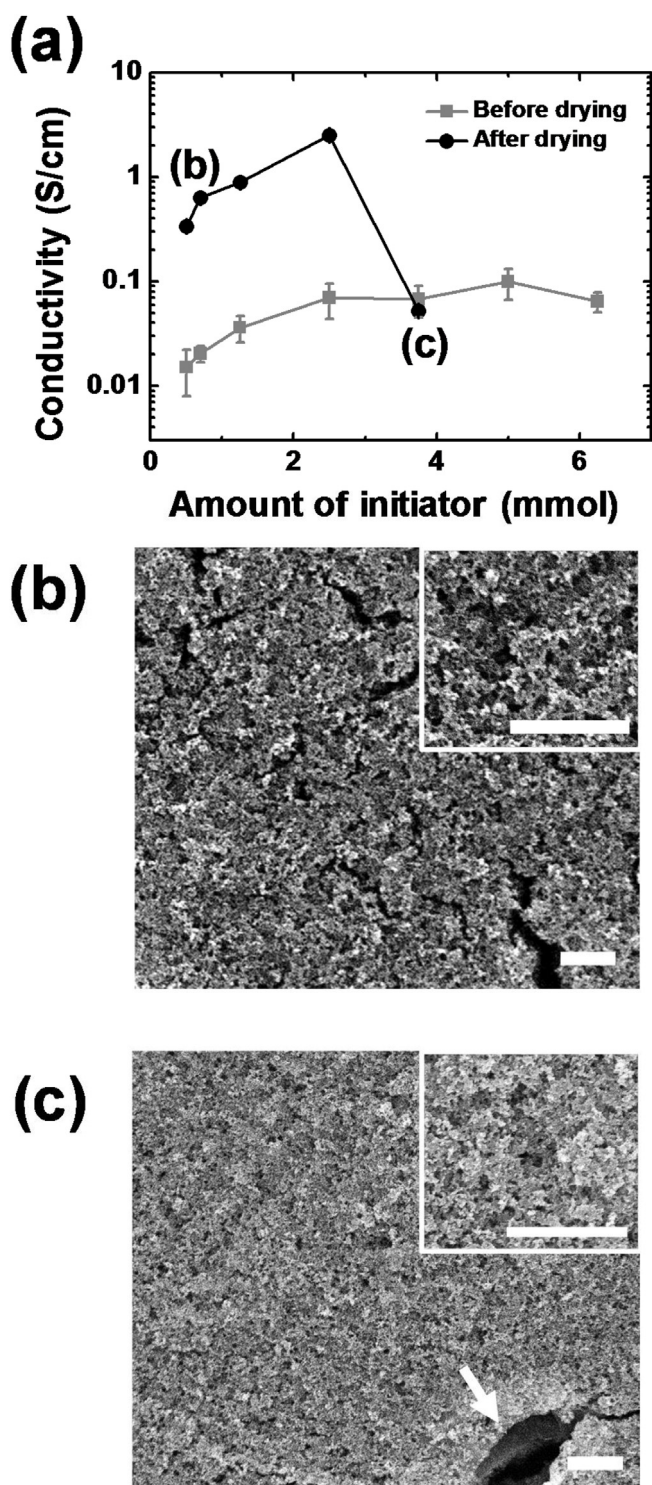
(a)

(b)

(c)

Fig. 6. Effect of the amount of the initiator, ammonium persulfate. (a) Conductivity of the PANI film with the amount of the initiator before (■) and after (●) the dehydration process. SEM images of the PANI films with the initiator of (b) 0.7 mmol and (c) 3.75 mmol, whose conductivity values are indicated in (a). The white arrow indicates the crack of the PANI film at the high initiator content. Scale bars = 10 μm in all images. All the porous PANI films were prepared with the 150 μm thick spacer, and then dried.

be easily deformed or damaged during fabrication and measurement.

Electrochemical impedance spectroscopy (EIS) measurements of the PANI electrodes prepared at the C 1.5 and the REF compositions were carried out to study the frequency responses

of electrodes over a frequency range of 10^6–10^{-2} Hz (Fig. 7 (b)). In the Nyquist plots, the intercept of the real component (Z_{re}) is commonly related to the equivalent series resistance (ESR), which is in turn associated with a combination of electrolyte, electrode, current collector, and the contact resistance between the electrode and current collector. The ESR of the C 1.5 electrode is 10 Ω, which is smaller than that of the REF electrode. Moreover, in the low-frequency region, the C 1.5 electrode exhibits a steeper slope with respect to the real axis (Z_{re}) than does the REF electrode, indicating more capacitive feature. This finding is further supported by the Bode plot (inset in Fig. 7 (b)). The phase angle of the C 1.5 composition in the low-frequency region ($\sim 10^{-2}$ Hz) is closer to 90°, which is indicative of an ideal capacitor, compared to the phase angle of the REF electrode [33,56]. Fig. 7 (c) shows plots of reciprocal of volumetric capacitance (1/C) against the square root of the scan rate for PANI electrodes prepared at the C 1.5 and the REF compositions. The y-intercepts were obtained from an extrapolated fitting line to the y-axis. The reciprocal y-intercept represents the "total capacitance", which is the capacitance value when the scan rate approaches 0 mV/s [57]. At this moment, the ions in the electrolyte are sufficiently filled in the entire electrode surface. The total capacitance of the REF and C 1.5 PANI were 459 F/cm^3 and 690 F/cm^3, respectively. It should be noted that in this study, the film is made of pure PANI without any conducting additives and/or binders and exhibits excellent volumetric capacitance, higher than that of other capacitors based on PANI composites. The CV curves of the PANI film (C 1.5, 250 μm thick) at various scan rates (10–200 mV/s) are shown in Fig. S4 (a). With increasing scan rates, the CV curves are slightly distorted due to the limited ion diffusion, but still present reasonable capacitive features up to 200 mV/s, demonstrating a fast charge response.

If the hierarchical pores in the PANI electrode are three-dimensionally distributed and well connected (i.e. open pore network), thicker PANI film can provide a more active surface area for electrochemical reactions. Fig. 7 (d) shows the areal capacitance of the PANI electrodes with different thicknesses. The areal capacitance increases from 253 to 704 mF/cm^2 when the thickness increases from 50 μm to 250 μm. This result is mainly attributed to the increased wetting of the thicker PANI electrode by electrolyte ions. When the thickness of the film increases to 350 μm, however, the areal capacitance was reduced to 497 mF/cm^2. The crack formation in the thick PANI film (>350 μm) during dehydration has been frequently observed (Fig. 2). These cracks cause destruction of the pore structure and a decrease in electrical conductivity. This crack formation likely causes the decreased capacitance in the 350 μm thick PANI film.

For further investigation of electrochemical performances, GCD profiles of the PANI electrodes with the C 1.5 and REF compositions were recorded at a constant current of 2.8 A/cm^3 (Fig. S5). The C 1.5 PANI electrode has a longer discharge time than that of the REF electrode, resulting in better capacitance. The potential-time response during a charge/discharge process of both PANI electrodes shows a nearly symmetric triangular shape with transitions, which is consistent with the CV results. The corresponding capacitance at 0.94 mA/cm^3 is 282 F/cm^3, which is comparable to the capacitance obtained from the CV curves. After 5000 GCD cycles at a constant current of 2.8 A/cm^3, the PANI electrode retains ~54% of its initial capacitance value (Fig. S5 (c)). It has been reported that conducting polymers, like PANI and polypyrrole (PPy), could undergo volumetric swelling and shrinking due to injection/rejection of electrolyte ions during repeated charge-discharge processes [57,58]. This likely leads to deteriorated conformation of π-conjugated PANI chains and decreases in capacitance [33].

Along with the three-electrode configuration, the two-electrode configuration could also be meaningful, especially for
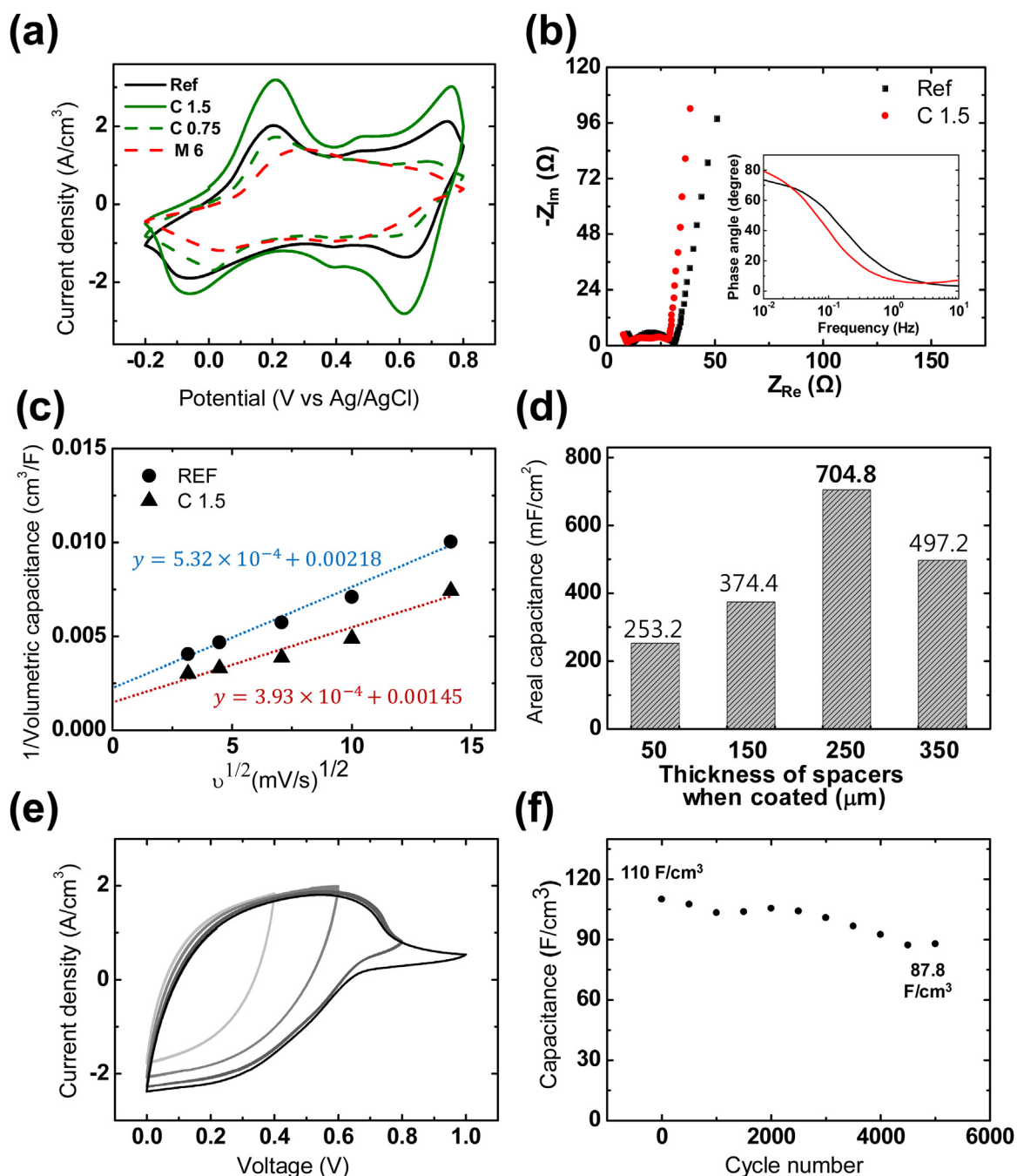
Fig. 7. (a–d) Electrochemical characteristics of a PANI electrode in a three-electrode configuration: (a) CV curves of the PANI electrodes prepared at selected preparation compositions at a constant scan rate of 10 mV/s over the potential window of −0.2 to 0.8 V. The PANI electrodes were labeled as shown in Table 1 depending on the preparation composition. (b) Nyquist plots for the PANI electrodes with the REF and C 1.5 compositions and the corresponding Bode plots (Inset). (c) Plots of reciprocal of volumetric capacitance (1/C) against square root of scan rate for the REF and C 1.5 PANI. (d) The capacitance values of a PANI electrode with different thicknesses. (e-f) Electrochemical characteristics of a supercapacitor composed of two symmetric PANI electrodes (2-electrode configuration): (e) CV curves at different voltage windows and (f) cycle stability of a two symmetric PANI electrode over 5000 GCD cycles at a constant current of 2.8 A/cm^3. The PANI electrodes for (d–f) were prepared at C1.5 composition.

practical device fabrication. We fabricated a symmetric capacitor with a pair of the C 1.5 PANI electrodes and conducted the electrochemical measurements. To determine the appropriate voltage window for charge-discharge operation, the CV curves were obtained while changing the voltage ranges at a constant scan rate of 50 mV/s (Fig. 7 (e)). The CV curve over the voltage window of 0–0.6 V shows a stable loop without notable polarization. At a slow scan rate of 10 mV/s, the C 1.5 electrode reveals a

rectangular CV curve, indicating ideal capacitive behavior due to fast charge propagation across electrodes (Fig. S6 (a)). We also investigated the effects of charge-discharge current density on the capacitance. (Fig. S6 (b)). The calculated volumetric capacitance is 278.9 F/cm^3 at a current density of 0.94 A/cm^3, but it decreases as the current density increases, down to 95.27 F/cm^3 at a current density of 3.75 A/cm^3. The cycle stability was investigated under the repeating GCD cycles at a constant charge-discharge current

Table 1
Sample labels for different compositions and their conductivity values, and volumetric capacitances in a 3-electrode configuration.

Labels of PANI compositions	Initiator (mmol)	Crosslinker (mmol)	Monomer (mmol)	Density (g/cm³)	Volumetric surface area (m²/cm³)[a]	Conductivity (S/cm)	Volumetric Capacitance (F/cm³)[b]
REF	1.25	1.0	5.0	0.849	21.65	0.90	247.01
C 0.75	1.25	0.75	5.0	0.677	22.16	0.21	182.85
C 1.5	1.25	1.5	5.0	1.373	25.38	1.79	330.85
M 2	1.25	1.0	2.0	1.397	25.75	3.44	not measurable
M 6	1.25	1.0	6.0	0.979	20.87	0.18	152.14

[a] The nitrogen adsorption–desorption isotherm is shown in Fig. S3.
[b] The capacitance values were calculated from CV curves in Fig. 7 (a).

density of 2.8 A/cm³. The capacitor with the symmetric C 1.5 PANI electrodes retains 80% of its initial capacitance (110 F/cm³) for 5000 GCD cycles, demonstrating a good cycle stability (Fig. 7 (f)).

Conclusion

In conclusion, we developed a facile process to fabricate a highly conducting porous polymer film based on a PANI hydrogel paste and systematically investigated the effects of the preparation composition of the gel paste on the morphology of the final polymer film. The PANI porous film is prepared by a doctor-blading technique and successive drying process. The dehydration of the PANI hydrogel film results in a highly dense, porous film, whose conductivity is drastically improved compared to the wet-state hydrogel film. Our study reveals that the composition used while preparing the PANI hydrogel paste has a considerable influence on the pore morphology and the resulting conductivity of the resulting PANI porous film. When the amount of crosslinker increases or the amount of monomer decreases, the porous morphology of the PANI film becomes dense and the conductivity increases. Even though little influence on the pore morphology and the conductivity due to the amount of initiator is observed, it is still a critical component in forming a mechanically stable PANI film after the drying process. The pore characterization by SEM, BET, and MIP reveals the formation of hierarchical pore structures in the resulting PANI films. Such a highly conducting, surface-active PANI film with hierarchical open pores could be an efficient electrode for electrochemical systems, such as pseudocapacitors. We conducted electrochemical measurements of the PANI electrode prepared at various compositions. It turns out that the composition, C 1.5, is optimal for the preparation of the PANI electrode with high conductivity and volumetric surface area, leading to excellent volumetric capacitance. The total volumetric capacitance of 690 F/cm³ was achieved, which is significantly higher than that of recently reported PANI-based capacitors. It should be noted that pure PANI was used without any conducting additives/binders in this study. The areal capacitance of the PANI electrode increases with thickness, presumably due to the three-dimensionally distributed open pores in the PANI electrode. Above 250 μm, the capacitance decreases because of crack formation during dehydration. Finally, we fabricated a symmetric capacitor with a pair of PANI electrodes, which could be a more practical device configuration. The capacitor exhibited a volumetric capacitance 110 F/cm³ at a current density of 2.8 A/cm³ and maintained 80% of its capacitance after 5000 charge/discharge cycles. The PANI film with well-defined open pores and electrochemically active surface by the simple method established in this study can be used for many electrochemical applications, such as energy storage devices and sensors.

Conflict of interest

None.

Acknowledgments

Appendix A. Supplementary data

Supplementary material related to this article can be found, in the online version, at doi:https://doi.org/10.1016/j.jiec.2020.02.013.

References

[1] W. Ma, C. Yang, X. Gong, K. Lee, A.J. Heeger, Adv. Funct. Mater. 15 (2005) 1617.
[2] Y. Liu, J. Zhao, Z. Li, C. Mu, W. Ma, H. Hu, K. Jiang, H. Lin, H. Ade, H. Yan, Nat. Commun. 5 (2014) 5293.
[3] G. Widawski, M. Rawiso, B. François, Nature 369 (1994) 387.
[4] S. Freiberg, X. Zhu, Int. J. Pharm. 282 (2004) 1.
[5] N.C. Abeykoon, J.S. Bonso, J.P. Ferraris, RSC Adv. 5 (2015) 19865.
[6] H. Zhu, Y. Li, N. Chen, C. Lu, C. Long, Z. Li, Q. Liu, J. Membrane Sci. 590 (2019) 117307.
[7] J. Zhou, G. Lubineau, ACS Appl. Mater. Inter. 5 (2013) 6189.
[8] H. Deng, L. Lin, M. Ji, S. Zhang, M. Yang, Q. Fu, Prog. Polym. Sci. 39 (2014) 627.
[9] F. Sugiyama, A.T. Kleinschmidt, L.V. Kayser, D. Rodriquez, M. Finn, M.A. Alkhadra, J.M.H. Wan, J. Ramírez, A.S.C. Chiang, S.E. Root, Polym. Chem-uk. 9 (2018) 4354.
[10] Y.H. Kim, C. Sachse, M.L. Machala, C. May, L. Müller-Meskamp, K. Leo, Adv. Funct. Mater. 21 (2011) 1076.
[11] L. Dai, B. Winkler, L. Dong, L. Tong, A.W. Mau, Adv. Mater. 13 (2001) 915.
[12] J.G. Hardy, D.J. Mouser, N. Arroyo-Currás, S. Geissler, J.K. Chow, L. Nguy, J.M. Kim, C.E. Schmidt, J. Mater. Chem. B. 2 (2014) 6809.
[13] E. Ochoteco, J.A. Pomposo, M. Bengoechea, H. Grande, J. Rodriguez, Polym. Advan. Technol. 18 (2007) 64.
[14] G. Pasparakis, T. Manouras, A. Selimis, M. Vamvakaki, P. Argitis, Angew. Chem. Int. Edit. 50 (2011) 4142.
[15] V. Vijayakumar, T.Y. Son, H.J. Kim, S.Y. Nam, J. Membrane Sci. 591 (2019)117314.
[16] T.N. Gao, T. Wang, W. Wu, Y. Liu, Q. Huo, Z.A. Qiao, S. Dai, Adv. Mater. 31 (2019) 1806254.
[17] J. Germain, J. Hradil, J.M. Fréchet, F. Svec, Chem. Mater 18 (2006) 4430.
[18] J. Germain, J.M. Fréchet, F. Svec, J. Mater. Chem. 17 (2007) 4989.
[19] Q. Hou, D.W. Grijpma, J. Feijen, J. Biomed. Mater. Res. B. 67 (2003) 732.
[20] J.W. Kim, K. Taki, S. Nagamine, M. Ohshima, Chem. Eng. Sci. 63 (2008) 3858.
[21] L. Jinhua, L. Dongliang, W. Honghua, Z. Guangyuan, Polymer 52 (2011) 602.
[22] I. Tsivintzelis, G. Sanxaridou, E. Pavlidou, C. Panayiotou, J. Supercrit. Fluid. 110 (2016) 240.
[23] Z. Xinli, H. Xiaoling, G. Ping, L. Guozheng, J. Supercrit. Fluid. 49 (2009) 111.
[24] X.Y. Yang, L.H. Chen, Y. Li, J.C. Rooke, C. Sanchez, B.L. Su, Chem. Soc. Rev. 46 (2017) 481.
[25] J. Zhang, C.M. Li, Chem. Soc. Rev. 41 (2012) 7016.
[26] Y. Wang, A.S. Angelatos, F. Caruso, Chem. Mater. 20 (2007) 848.
[27] A. Eftekhari, Nanostructured Conductive Polymers, Wiley, 2011.
[28] D. Zhai, B. Liu, Y. Shi, L. Pan, Y. Wang, W. Li, R. Zhang, G. Yu, ACS Nano 7 (2013) 3540.
[29] J. Jang, J. Ha, J. Cho, Adv. Mater. 19 (2007) 1772.
[30] X. Yan, J. Chen, J. Yang, Q. Xue, P. Miele, ACS Appl. Mater. Inter. 2 (2010) 2521.
[31] K. Zhang, L.L. Zhang, X. Zhao, J. Wu, Chem. Mater. 22 (2010) 1392.
[32] L. Liu, Z. Niu, L. Zhang, W. Zhou, X. Chen, S. Xie, Adv. Mater. 26 (2014) 4855.
[33] M. Umashankar, S. Palaniappan, RSC Adv. 5 (2015) 70675.
[34] Q. Li, J. Wu, Q. Tang, Z. Lan, P. Li, J. Lin, L. Fan, Electrochem. Commun. 10 (2008) 1299.
[35] C. Dhand, M. Das, M. Datta, B. Malhotra, Biosens. Bioelectron. 26 (2011) 2811.

[36] L. Pan, G. Yu, D. Zhai, H.R. Lee, W. Zhao, N. Liu, H. Wang, B.C.K. Tee, Y. Shi, Y. Cui, PNAS 109 (2012) 9287.

[37] X. He, C. Zhang, M. Wang, Y. Zhang, L. Liu, W. Yang, ACS Appl. Mater. Inter. 9 (2017) 11134.

[38] Y. Wu, Y.X. Chen, J. Yan, D. Quinn, P. Dong, S.W. Sawyer, P. Soman, Acta. Biomater. 33 (2016) 122.

[39] J. Suriboot, Y. Hu, T.J. Malinski, H.S. Bazzi, D.E. Bergbreiter, ACS Omega 1 (2016) 714.

[40] S. Ahmadjo, Polym. Advan. Technol. 27 (2016) 1523.

[41] P.J. Flory, Principles of Polymer Chemistry, Cornell University Press, 1953.

[42] J.M. Harris, Poly (ethylene glycol) Chemistry: Biotechnical and Biomedical Applications, Springer Science & Business Media, New York, 1992.

[43] W.F. Su, Principles of Polymer Design and Synthesis, Springer, 2013.

[44] E. Song, J.W. Choi, Nanomaterials 3 (2013) 498.

[45] V.H.R. de Souza, M.M. Oliveira, A.J.G. Zarbin, J. Power Sources 260 (2014) 34.

[46] D.W. Wang, F. Li, J. Zhao, W. Ren, Z.G. Chen, J. Tan, Z.S. Wu, I. Gentle, G.Q. Lu, H. M. Cheng, ACS Nano 3 (2009) 1745.

[47] X. Lu, H. Dou, S. Yang, L. Hao, L. Zhang, L. Shen, F. Zhang, X. Zhang, Electrochim. Acta 56 (2011) 9224.

[48] H. Heydari, M.B. Gholivand, New J. Chem. 41 (2017) 237.

[49] Z. Niu, W. Zhou, X. Chen, J. Chen, S. Xie, Adv. Mater. 27 (2015) 6002.

[50] J. Yan, Q. Wang, C. Lin, T. Wei, Z. Fan, Adv. Energy Mater. 4 (2014)1400500.

[51] M.N. Hyder, S.W. Lee, F.Ç. Cebeci, D.J. Schmidt, Y. Shao-Horn, P.T. Hammond, ACS Nano 5 (2011) 8552.

[52] H. Itoi, S. Maki, T. Ninomiya, H. Hasegawa, H. Matsufusa, S. Hayashi, H. Iwata, Y. Ohzawa, Nanoscale 10 (2018) 9760.

[53] N. Hu, L. Zhang, C. Yang, J. Zhao, Z. Yang, H. Wei, H. Liao, Z. Feng, A. Fisher, Y. Zhang, Sci. Rep. 6 (2016) 19777.

[54] Y. Wang, X. Yang, A.G. Pandolfo, J. Ding, D. Li, Adv. Energy Mater. 6 (2016) 1600185.

[55] J. Pedrós, A. Boscá, J. Martínez, S. Ruiz-Gómez, L. Pérez, V. Barranco, F. Calle, J. Power Sources 317 (2016) 35.

[56] M.E. Orazem, N. Pébère, B. Tribollet, J. Electrochem. Soc. 153 (2006) B129.

[57] T. Liu, L. Finn, M. Yu, H. Wang, T. Zhai, X. Lu, Y. Tong, Y. Li, Nano Lett. 14 (2014) 2522.

[58] Y. Tao, Z. Liu, X.-Z. Song, M. Bao, Z. Tan, Nano 12 (2017)1750088.